Supporting Information

A Porous Coordination Polymer Showing Guest-Amplified Positive and Negative Thermal Expansion

Zi-Ming Ye†, Kai-Ping Xie†, Chao Wang†, Xue-Wen Zhang†, Hao-Long Zhou‡*, and Jie-Peng Zhang†*

†MOE Key Laboratory of Bioinorganic and Synthetic Chemistry, School of Chemistry, Sun Yat-Sen University, Guangzhou 510275, China

‡Department of Chemistry and Key Laboratory for Preparation and Application of Ordered Structural Materials of Guangdong Province, Shantou University, Shantou 515063, China

E-mail: zhangjp7@mail.sysu.edu.cn, hlzhou@stu.edu.cn

1 Experimental Section

1.1 Materials and instruments

All reagents were commercially available and used without purification except otherwise specified. 4-(1*H*-pyrazol-4-yl)benzoic acid (H_2pba) was synthesized according to the literature method.[1] Elemental analyses (EA) were performed on a Vario EL elemental analyzer. Powder X-ray diffraction (PXRD) data were obtained by a Bruker D8 ADVANCE/DISCOVER X-ray powder diffractometer (Cu Kα). Thermogravimetry analyses were conducted on a TA Q50 instrument under N_2 atmosphere with a heating rate of 10.0 K/min. Gas adsorption isotherms were collected on a Micrometrics ASAP 2020M instrument. Before gas adsorption experiment, the sample (ca. 100 mg) was placed in the sample tube and heated under high vacuum at 523 K to remove the remnant guest molecules.

1.2 Synthesis

$Zn(NO_3)_2{\cdot}6H_2O$ (60 mg, 0.2 mmol) and H_2pba (37.6 mg, 0.2 mmol) were dissolved in a mixture of DMA (1.5 mL), MeOH (4 mL) and toluene (Tol, 1.5 mL). Then the solution was sealed in a 15-mL Teflon reactor and heated at 393 K for 3 days. After cooling to room temperature at a rate of 10 K/h, prism-shaped crystals of [Zn(pba)]·0.5Tol (**1·t**) were filtered, washed by Tol, and dried in air (yield ~70%). The crystals of **1·t** were heated at 523 K for 180 minutes under nitrogen flow or vacuum to give [Zn(pba)] (**1**). EA calculated (%) for [Zn(pba)]·0.5H_2O ($C_{10}H_7N_2O_{2.5}Zn$): C 46.10, H 2.71, N 10.75; found C 45.94, H 2.52, N 10.76.

1.3 Single-crystal X-ray diffraction

Single-crystal X-ray diffraction (SCXRD) data were collected on a Bruker D8 QUEST diffractometer (Mo Kα). The data collection and reduction were carried out using the Bruker APEX3 program. The specimen of [Zn(pba)] was sealed in a glass capillary under vaccum. The test temperature was controlled by dry N_2 open flow using an Oxford Cryosystem K450 cooler system, and corrected by a thermal couple. The structures were solved by the direct method and refined by the full-matrix least squares method on F^2 using the SHELXTL software package in OLEX2. Anisotropic thermal parameters were used to refine all non-hydrogen atoms. Hydrogen atoms were generated geometrically.

2 Figures and Tables

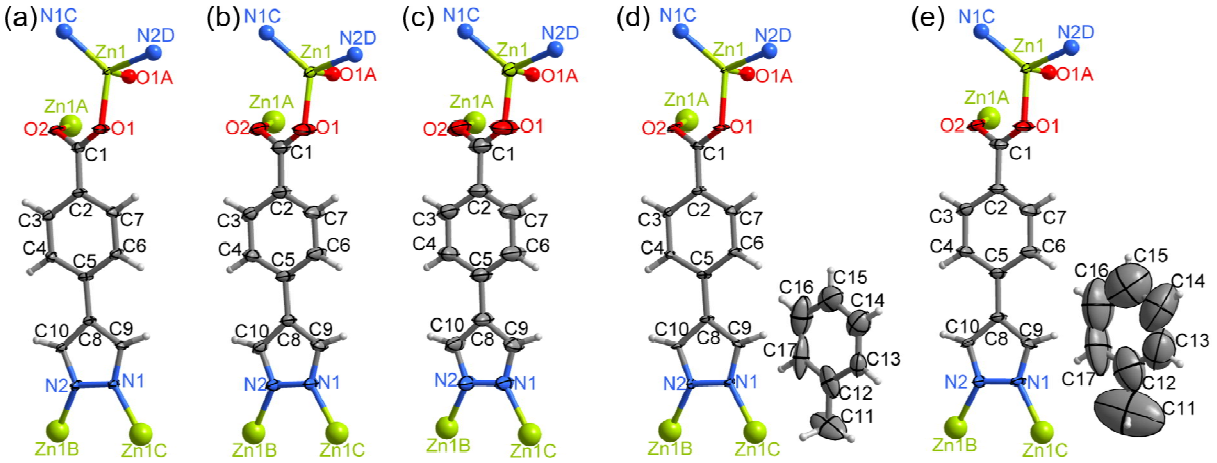

Figure S1. The asymmetric units of **1** at (a) 148 K, (b) 298 K and (c) 473 K and **1·t** at (d) 148 K and (e) 298 K. A = 1-*x*, *y*, 3/2-*z*; B = 1/2+*x*, 1/2-*y*, -1/2+*z*; C = 3/2-*x*, 1/2+*y*, 3/2-*z*; D = -1/2+*x*, 1/2-*y*, 1/2+*z*.

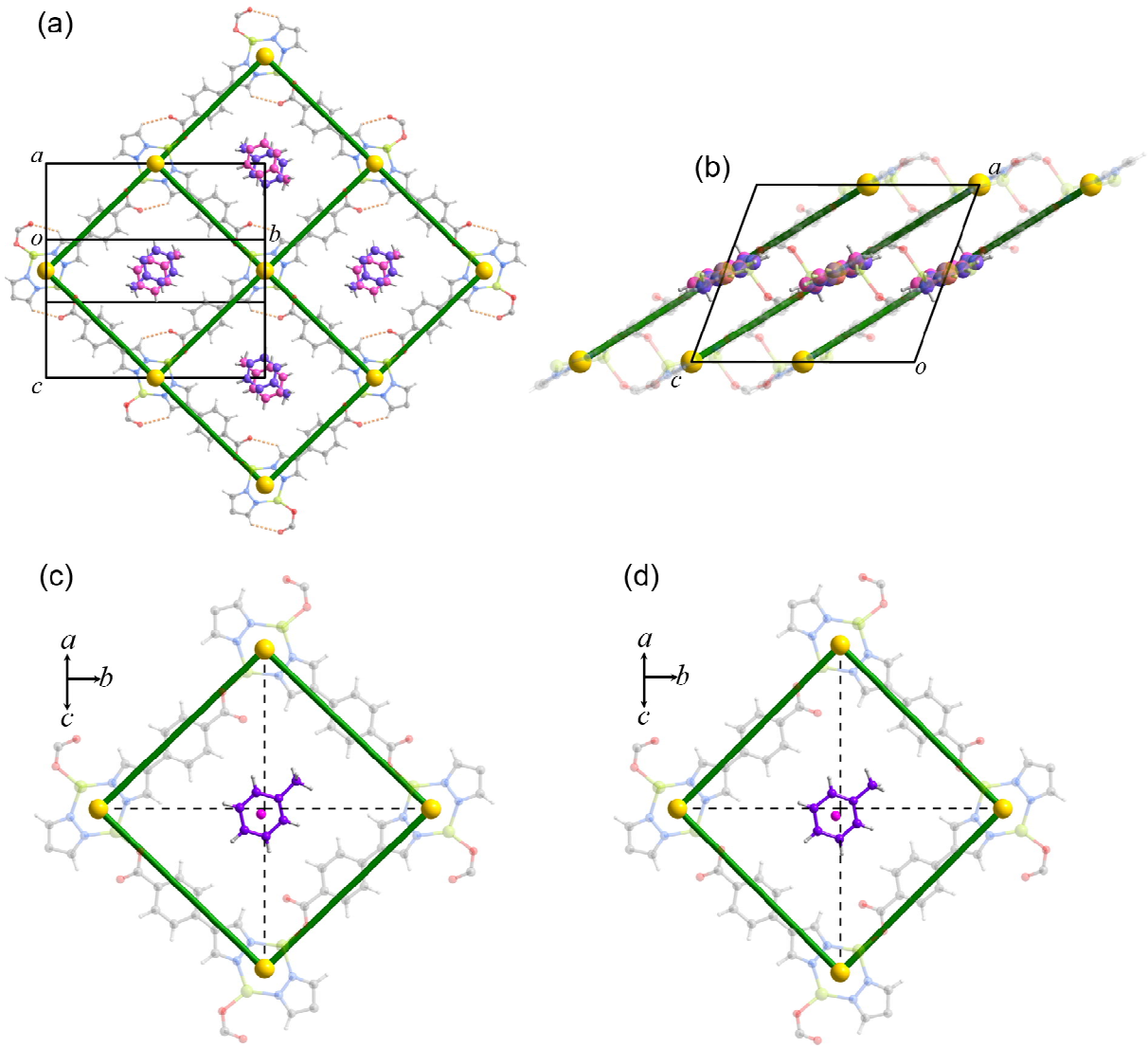

Figure S2. (a) Top and (b) side views of the loacations of Tol guests in the **sql** layers of **1**·**t** at 298 K (Two-fold symmetric disordered Tol guests are shown in pink and violet, respectivley). Displacement of phenyl ring center of Tol (pink sphere) from the grid center of the **sql** net (black cross) at (c) 148 K and (d) 298 K in **1**·**t**.

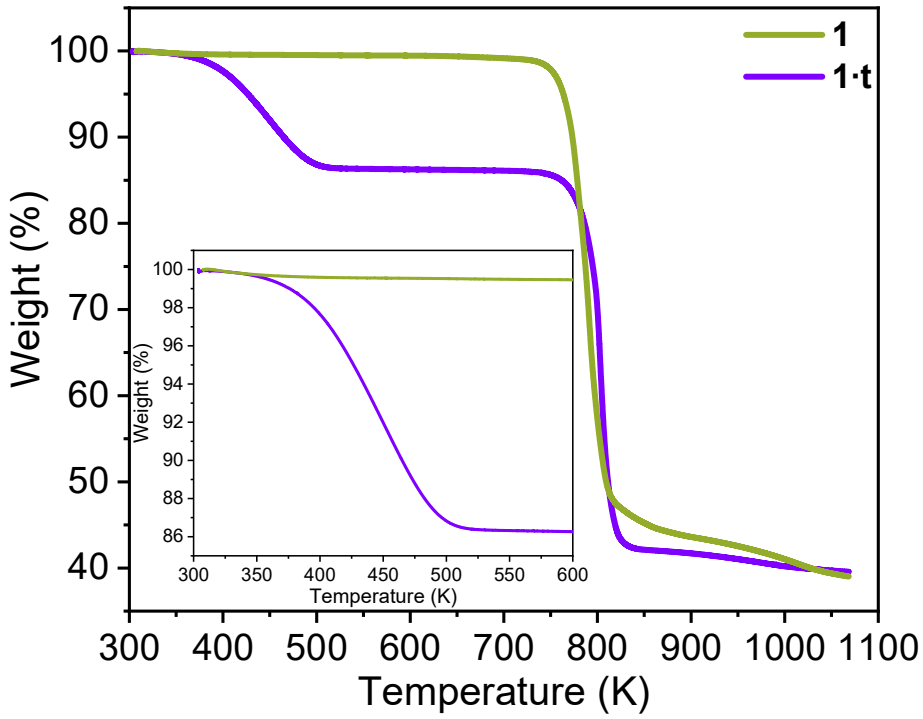

Figure S3. Thermogravimetry curves of **1** and **1·t**.

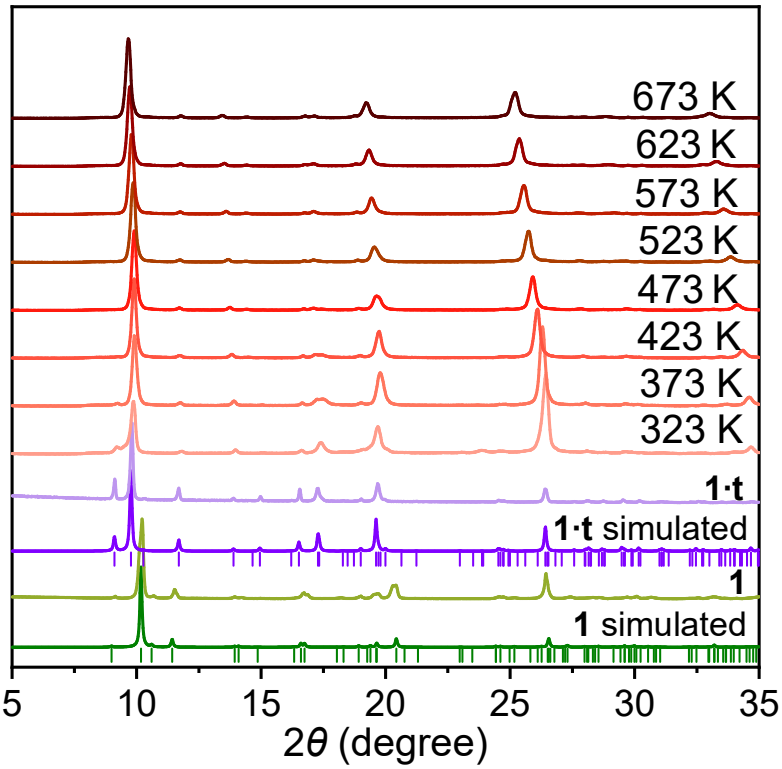

Figure S4. PXRD patterns of **1** at 298 K and variable-temperature PXRD patterns of **1·t**.

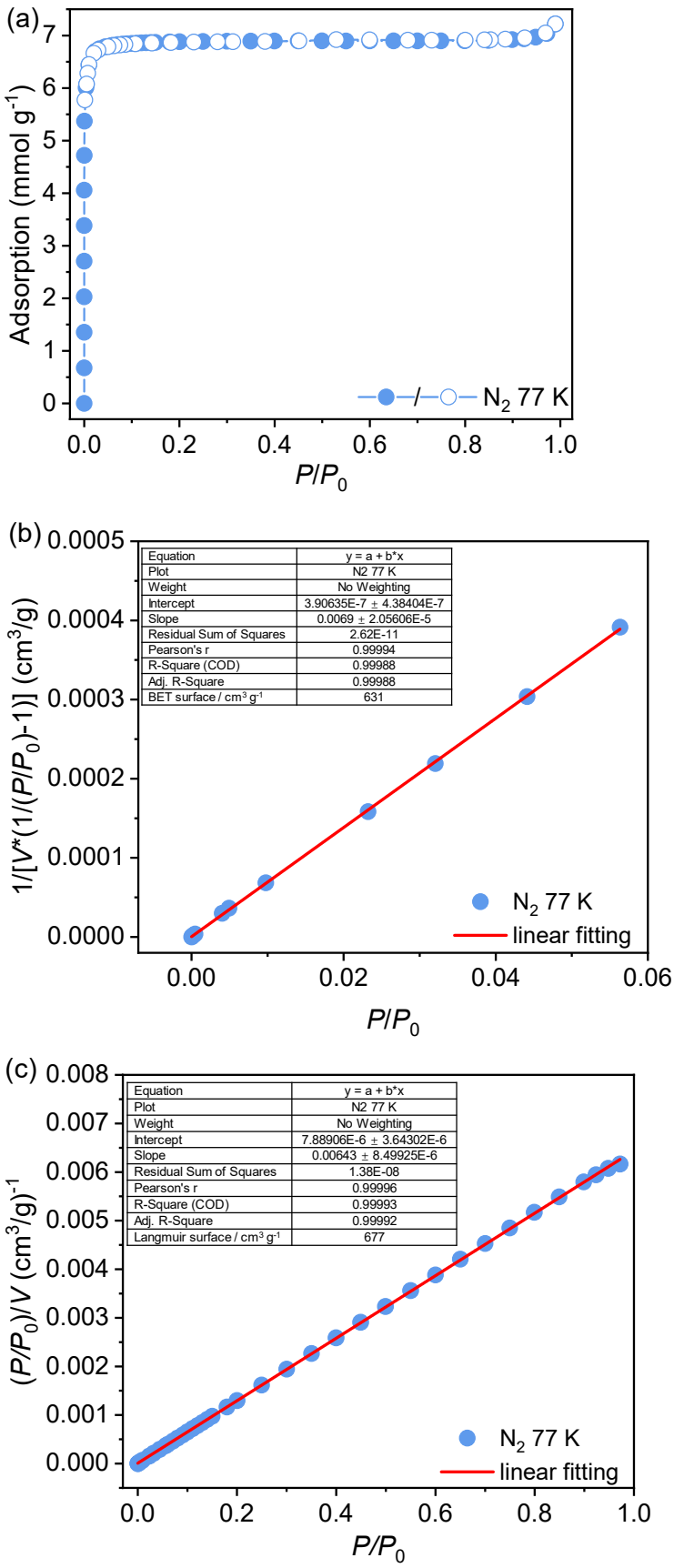

Figure S5. (a) N_2 (77 K) adsorption (solid) and desorption (open) isotherms of **1**. (b) BET and (c) Langmuir fitting results of the adsorption isotherm.

Table S1. Crystallographic data and structure refinement details.

Complex	**1**	**1**	**1**	**1·t**	**1·t**
Formula	$C_{10}H_6ZnN_2O_2$	$C_{10}H_6ZnN_2O_2$	$C_{10}H_6ZnN_2O_2$	$C_{13.5}H_{10}ZnN_2O_2$	$C_{13.5}H_{10}ZnN_2O_2$
Formula weight	251.56	251.56	251.56	297.60	297.60
Temperature (K)	148(1)	298(1)	473(1)	148(1)	298(1)
Crystal system	Monoclinic	Monoclinic	Monoclinic	Monoclinic	Monoclinic
Space group	*C*2/*c*	*C*2/*c*	*C*2/*c*	*C*2/*c*	*C*2/*c*
a/Å	9.7597(4)	10.2098(7)	10.7561(9)	9.9441(7)	10.8866(10)
b/Å	19.8289(7)	19.6476(11)	19.4423(15)	19.8552(13)	19.3940(16)
c/Å	13.3794(4)	13.2368(7)	13.0721(9)	13.2246(8)	12.8591(10)
β/°	108.657(2)	108.476(3)	108.065(4)	109.497(2)	110.104(3)
V/Å^3	2453.17(15)	2518.4(3)	2598.9(4)	2461.4(3)	2549.6(4)
Z	8	8	8	8	8
D_c/g cm^{-3}	1.362	1.327	1.286	1.606	1.551
reflns coll.	9044	9209	6721	8500	7872
unique reflns	2410	2479	2545	2426	2502
R_{int}	0.0441	0.0932	0.0681	0.0529	0.0596
R_1 [$I > 2\sigma(I)$][a]	0.0265	0.0345	0.0381	0.0410	0.0447
wR_2 [$I > 2\sigma(I)$][b]	0.0545	0.0752	0.0720	0.0710	0.0839
R_1 (all data)	0.0409	0.0593	0.0796	0.0562	0.0723
wR_2 (all data)	0.0587	0.0843	0.0849	0.0746	0.0934
GOF	1.046	1.025	1.038	1.083	1.063
Void ratio[c]/%	33.2	34.9	36.4	33.4	35.9
D_c(guest-free)/g cm^{-3}	1.362	1.327	1.286	1.358	1.311
Pore Volume/cm^3 g^{-1}	0.244	0.263	0.283	0.246	0.274

[a] $R_1=\sum||F_o|-|F_c||/\sum|F_o|$

[b] $wR_2=[\sum w(F_o^2-F_c^2)^2/\sum w(F_o^2)^2]^{1/2}$

[c] Calculated by PLATON using probe radius of 1.1 Å

Table S2. The variable-temperature unit-cell parameters of **1.**

T/K	*a*/Å	*b*/Å	*c*/Å	*β*/°	*V*/Å^3
148	9.7597(4)	19.8289(7)	13.3794(4)	108.657(2)	2453.17(15)
173	9.8167(5)	19.8024(10)	13.3629(6)	108.612(2)	2461.8(2)
198	9.8800(6)	19.7783(10)	13.3447(6)	108.556(2)	2472.1(2)
223	9.9490(6)	19.7447(10)	13.3195(6)	108.514(2)	2481.1(2)
248	10.0284(6)	19.7099(10)	13.2951(7)	108.496(2)	2492.2(2)
273	10.1198(6)	19.6761(11)	13.2626(7)	108.492(2)	2504.5(2)
298	10.2098(7)	19.6476(11)	13.2368(7)	108.476(3)	2518.4(3)
323	10.3005(6)	19.6143(10)	13.2056(6)	108.466(2)	2530.6(2)
348	10.3873(7)	19.5764(11)	13.1753(7)	108.446(2)	2541.5(3)
373	10.4741(7)	19.5444(11)	13.1504(7)	108.398(3)	2554.4(3)
398	10.5521(7)	19.5155(12)	13.1273(7)	108.337(3)	2566.0(3)
423	10.6260(8)	19.4911(12)	13.1067(7)	108.274(3)	2577.7(3)
448	10.6918(8)	19.4641(13)	13.0864(8)	108.177(3)	2587.5(3)
473	10.7561(9)	19.4423(15)	13.0721(9)	108.065(4)	2598.9(4)

Table S3. The variable-temperature unit-cell parameters of **1·t.**

T/K	*a*/Å	*b*/Å	*c*/Å	*β*/°	*V*/Å^3
148	9.9441(7)	19.8552(13)	13.2246(8)	109.497(2)	2461.4(3)
160.5	9.9898(7)	19.8324(13)	13.2166(9)	109.497(2)	2468.3(3)
173	10.0376(8)	19.7976(14)	13.2030(9)	109.502(3)	2473.2(3)
185.5	10.0885(8)	19.7715(14)	13.1913(9)	109.510(3)	2480.1(3)
198	10.1755(8)	19.7376(14)	13.1677(9)	109.578(3)	2491.7(3)
210.5	10.2526(8)	19.6966(14)	13.1367(9)	109.650(3)	2498.4(3)
223	10.3506(8)	19.6538(15)	13.0988(10)	109.751(3)	2507.9(4)
235.5	10.4477(9)	19.6031(15)	13.0539(10)	109.862(3)	2514.5(4)
248	10.5607(9)	19.5538(16)	13.0026(10)	109.984(3)	2523.4(4)
260.5	10.6612(10)	19.4969(16)	12.9511(10)	110.086(3)	2528.3(4)
273	10.7479(10)	19.4519(15)	12.9100(10)	110.144(3)	2534.0(4)
285.5	10.8216(10)	19.4163(15)	12.8779(10)	110.140(3)	2540.4(4)
298	10.8866(10)	19.3940(16)	12.8591(10)	110.104(3)	2549.6(4)

Table S4. Relationship of crystallography axes and PASCal calculated principal axes.

	Principal axis	Directions	Component of principal axis along		
			a	*b*	*c*
1	*a′*	~*a*	-0.9897	0	-0.1435
	b′	*b*	0	1	0
	c′	~*c*	-0.1755	0	-0.9845
1·t	*a′*	~*a*	-0.9946	0	-0.1034
	b′	*b*	0	1	0
	c′	~*c*	0.2636	0	0.9646

Table S5. Exceptionally large axial PTE/NTE coefficients of crystalline materials.

Compound	α_{PTE}/MK^{-1}	α_{NTE}/MK^{-1}	T/K	Ref.
1	347	-63/-83	148-473	This Work
1·t	689	-171/-249	148-298	
FJ1-H11-Me	653	-38/-38	100-293	2
MCF-82	482/61	-218	112-300	3
MCF-18·DMF	437	NA/NA	119-295	4
MCF-44	381/28	-148	144-278	5
SION-2	230/43	-153	100-340	6
FMOF-1	230/230	-170	90-295	7
Ag(tcm)	200	-54/-48	100-250	8
HMOF-1	177/3	-21	160-320	9
$[Zn(L)_2(OH)_2]\cdot MeOH$	166	-41/-41	100-295	10
$[Zn(FMA)(BPA)]\cdot H_2O$	157/55	-117	100-240	11
$Ag_3[Co(CN)_6]$	150/150	-130	20-496	12
Ag(mim)	130/44	-25	20-300	13
$[Cu(bpy)_2(OTf)_2]$	79	-21/21	133-383	14
$Cd(eim)_2$	66/66	-55	123-473	15
MCF-34·DMF	152/16 4075 258/218/74 237/36	-56 -3367/-3 / -116	127-208 208-215* 215-233 233-299	16
$[Zn_2(fu\text{-}L^1)_2(dabco)]$	≤1161/≤1611	≥-380	303-463	17
$\{[FeTp(CN)_3]_2Co(Bib)_2\}\cdot 5H_2O$	77/58 1089/278/85 110/66 197	-10 / -9 -656/-18	90-180 180-240*[a] 240-300 300-350*[b]	18
[Cu(tcm)]	591	-407/NA	20-240*[c]	19
$(Himd)_2[CuCl_4]$	568	-184/-34	273-353	20
(S,S)-Octa-3,5-diyn-2,7-diol	≤515	≥-85/-204	225-330	21
$CD_3OD\cdot D_2O$	462/93	-61	4-160	22
$C_{12}H_{24}O_6\cdot 2CH_3NO_2$	369/215	-198	180-273	23
CA-Pyz	1524/196	-1375	250-300*[d]	24
$[(H_4BPTC)(BPE)_2]$	≤814	≥-469/NA	333-408	25
BHH-BTBT	≤634/NA	≥-333	95-295*[e]	26
IMACET	226/239	-290	298-373	27

Coordination polymers and molecular crystals are grouped in blue and orange background, respectively.

* There is phase transition. [a] at 220/226 K; [b] at 310/322 K; [c] at 240 K; [d] at 300 K; [e] at 210 K.

Table S6. Key framework deformation parameters.

	1			**1·t**	
T	148 K	298 K	473 K	148 K	298 K
ω/°	60.74	59.55	58.07	60.46	58.37
θ_P/°	130.00	127.53	124.51	129.45	124.41
θ_L/°	92.70	91.60	90.32	92.48	89.70
L_P/Å	10.9395	10.9522	10.9838	10.9784	10.9618
L_L/Å	13.7021	13.7034	13.7093	13.7458	13.7499
Δ_{Off}/period	0.309	0.299	0.287	0.303	0.281

Table S7. The change of key framework deformation parameters from **1** to **1·t**.

	148 K			298 K		
Guest	None	Tol	Δ	None	Tol	Δ
ω/°	60.74	60.46	-0.28	59.55	58.37	-1.18
θ_P/°	130.00	129.45	-0.55	127.53	124.41	-3.12
θ_L/°	92.70	92.48	-0.22	91.60	89.70	-1.90
L_P/Å	10.9395	10.9784	+0.0389	10.9522	10.9618	+0.0096
L_L/Å	13.7021	13.7458	+0.0437	13.7034	13.7499	+0.0465
Δ_{Off}/period	0.309	0.303	-0.006	0.299	0.281	-0.018

Table **S8.** The change of key framework deformation parameters from 148 K to 298 K.

	1			**1·t**		
T	148 K	298 K	Δ	148 K	298 K	Δ
ω/°	60.74	59.55	-1.19	60.46	58.37	-2.09
θ_P/°	130.00	127.53	-2.47	129.45	124.41	-5.04
θ_L/°	92.70	91.60	-1.10	92.48	89.70	-2.78
L_P/Å	10.9395	10.9522	+0.0127	10.9784	10.9618	-0.0166
L_L/Å	13.7021	13.7034	+0.0013	13.7458	13.7499	+0.0041
Δ_{Off}/period	0.309	0.299	-0.010	0.303	0.281	-0.022

Table S9. Local connectivity geometries.

	1			**1·t**	
T	148 K	298 K	473 K	148 K	298 K
Zn1–O1/Å	1.9560(16)	1.956(2)	1.960(2)	1.958(2)	1.963(3)
Zn1–O2/Å	2.0206(16)	2.024(2)	2.028(3)	2.033(2)	2.032(3)
Zn1–N1/Å	1.9553(17)	1.958(2)	1.959(2)	1.952(2)	1.956(3)
Zn1–N1/Å	1.9771(17)	1.975(2)	1.973(2)	1.976(3)	1.976(3)
N1–Zn1–N2/°	111.21(7)	111.18(9)	111.32(9)	110.51(10)	110.90(12)
O1–Zn1–O2/°	99.19(6)	99.75(9)	100.42(11)	96.57(9)	98.12(12)
O1–Zn1–N1/°	124.59(8)	124.15(10)	123.65(12)	126.45(11)	125.26(13)
O1–Zn1–N2/°	104.51(7)	104.99(9)	105.24(10)	104.71(10)	105.54(12)
O2–Zn1–N1/°	107.27(7)	107.40(9)	107.80(11)	108.46(10)	108.48(12)
O2–Zn1–N2/°	108.81(7)	108.05(9)	106.95(11)	108.48(10)	106.67(12)
Zn1–O1–C1/°	115.71(10)	115.11(21)	114.130(25)	114.42(23)	112.54(26)
Zn1–O2–C1/°	122.23(14)	122.67(18)	123.80(23)	121.88(22)	122.76(23)
Zn1–N1–N2/°	120.30(12)	120.34(16)	120.48(18)	119.89(18)	119.99(21)
Zn1–N2–N1/°	122.61(13)	122.84(16)	122.59(21)	123.51(20)	123.02(27)
COO–Ph/°	21.06(23)	21.07(30)	21.78(38)	18.49(36)	19.89(43)
Pz–Ph/°	0.96(19)	0.61(26)	1.23(43)	2.47(25)	2.24(37)

COO = carboxylate group, Pz = pyrazolate ring, Ph = phenyl ring.

Table S10. The change of local connectivity geometries from **1** to **1·t**.

	148 K			298 K		
Guest	None	Tol	*Δ*	None	Tol	*Δ*
Zn1–O1/Å	1.9560(16)	1.958(2)	+0.0020	1.956(2)	1.963(3)	+0.007
Zn1–O2/Å	2.0206(16)	2.033(2)	+0.0124	2.024(2)	2.032(3)	+0.008
Zn1–N1/Å	1.9553(17)	1.952(2)	–0.0033	1.958(2)	1.956(3)	–0.002
Zn1–N1/Å	1.9771(17)	1.976(3)	–0.0011	1.975(2)	1.976(3)	+0.001
N1–Zn1–N2/°	111.21(7)	110.51(10)	–0.70	111.18(9)	110.90(12)	–0.28
O1–Zn1–O2/°	99.19(6)	96.57(9)	–2.62	99.75(9)	98.12(12)	–1.63
O1–Zn1–N1/°	124.59(8)	126.45(11)	+1.86	124.15(10)	125.26(13)	+1.11
O1–Zn1–N2/°	104.51(7)	104.71(10)	+0.20	104.99(9)	105.54(12)	+0.55
O2–Zn1–N1/°	107.27(7)	108.46(10)	+1.19	107.40(9)	108.48(12)	+1.08
O2–Zn1–N2/°	108.81(7)	108.48(10)	–0.33	108.05(9)	106.67(12)	–1.38
Zn1–O1–C1/°	115.71(10)	114.42(23)	–1.29	115.11(21)	112.54(26)	–2.57
Zn1–O2–C1/°	122.23(14)	121.88(22)	–0.35	122.67(18)	122.76(23)	+0.09
Zn1–N1–N2/°	120.30(12)	119.89(18)	–0.41	120.34(16)	119.99(21)	–0.35
Zn1–N2–N1/°	122.61(13)	123.51(20)	+0.90	122.84(16)	123.02(27)	+0.18
COO–Ph/°	21.06(23)	18.49(36)	–2.57	21.07(30)	19.89(43)	–1.18
Pz–Ph/°	0.96(19)	2.47(25)	+1.51	0.61(26)	2.24(37)	+1.63

COO = carboxylate group, Pz = pyrazolate ring, Ph = phenyl ring.

Table S11. The change of local connectivity geometries from 148 K to 298 K.

	1			**1·t**		
T	148 K	298 K	*Δ*	148 K	298 K	*Δ*
Zn1–O1/Å	1.9560(16)	1.956(2)	+0.000	1.958(2)	1.963(3)	+0.005
Zn1–O2/Å	2.0206(16)	2.024(2)	+0.003	2.033(2)	2.032(3)	–0.001
Zn1–N1/Å	1.9553(17)	1.958(2)	+0.003	1.952(2)	1.956(3)	+0.004
Zn1–N1/Å	1.9771(17)	1.975(2)	–0.002	1.976(3)	1.976(3)	+0.000
N1–Zn1–N2/°	111.21(7)	111.18(9)	–0.03	110.51(10)	110.90(12)	+0.39
O1–Zn1–O2/°	99.19(6)	99.75(9)	+0.56	96.57(9)	98.12(12)	+1.55
O1–Zn1–N1/°	124.59(8)	124.15(10)	–0.44	126.45(11)	125.26(13)	–1.19
O1–Zn1–N2/°	104.51(7)	104.99(9)	+0.48	104.71(10)	105.54(12)	+0.83
O2–Zn1–N1/°	107.27(7)	107.40(9)	+0.13	108.46(10)	108.48(12)	+0.02
O2–Zn1–N2/°	108.81(7)	108.05(9)	–0.76	108.48(10)	106.67(12)	–1.81
Zn1–O1–C1/°	115.71(10)	115.11(21)	–0.60	114.42(23)	112.54(26)	–1.88
Zn1–O2–C1/°	122.23(14)	122.67(18)	+0.44	121.88(22)	122.76(23)	+0.88
Zn1–N1–N2/°	120.30(12)	120.34(16)	+0.04	119.89(18)	119.99(21)	+0.10
Zn1–N2–N1/°	122.61(13)	122.84(16)	+0.23	123.51(20)	123.02(27)	–0.49
COO–Ph/°	21.06(23)	21.07(30)	+0.01	18.49(36)	19.89(43)	+1.40
Pz–Ph/°	0.96(19)	0.61(26)	–0.35	2.47(25)	2.24(37)	–0.23

COO = carboxylate group, Pz = pyrazolate ring, Ph = phenyl ring.

3 Reference

(1) Padial, N. M.; Quartapelle Procopio, E.; Montoro, C.; López, E.; Oltra, J. E.; Colombo, V.; Maspero, A.; Masciocchi, N.; Galli, S.; Senkovska, I.; Kaskel, S.; Barea, E.; Navarro, J. A. R., Highly Hydrophobic Isoreticular Porous Metal–Organic Frameworks for the Capture of Harmful Volatile Organic Compounds. *Angew. Chem. Int. Ed.* **2013**, *52*, 8290-8294.

(2) Pang, J.; Liu, C.; Huang, Y.; Wu, M.; Jiang, F.; Yuan, D.; Hu, F.; Su, K.; Liu, G.; Hong, M., Visualizing the Dynamics of Temperature- and Solvent-Responsive Soft Crystals. *Angew. Chem. Int. Ed.* **2016**, *55*, 7478-7482.

(3) Zhou, H.-L.; Zhang, Y.-B.; Zhang, J.-P.; Chen, X.-M., Supramolecular-jack-like guest in ultramicroporous crystal for exceptional thermal expansion behaviour. *Nat. Commun.* **2015**, *6*, 6917.

(4) Wei, Y.-S.; Chen, K.-J.; Liao, P.-Q.; Zhu, B.-Y.; Lin, R.-B.; Zhou, H.-L.; Wang, B.-Y.; Xue, W.; Zhang, J.-P.; Chen, X.-M., Turning on the flexibility of isoreticular porous coordination frameworks for drastically tunable framework breathing and thermal expansion. *Chem. Sci.* **2013**, *4*, 1539-1546.

(5) Zhou, H.-L.; Li, M.; Li, D.; Zhang, J.-P.; Chen, X.-M., Thermal expansion behaviors of Mn(II)-pyridylbenzoate frameworks based on metal-carboxylate chains. *Sci. China Chem.* **2014**, *57*, 365-370.

(6) Gładysiak, A.; Moosavi, S. M.; Sarkisov, L.; Smit, B.; Stylianou, K. C., Guest-dependent negative thermal expansion in a lanthanide-based metal–organic framework. *CrystEngComm* **2019**, *21*, 5292-5298.

(7) Yang, C.; Wang, X.; Omary, M. A., Crystallographic Observation of Dynamic Gas Adsorption Sites and Thermal Expansion in a Breathable Fluorous Metal–Organic Framework. *Angew. Chem. Int. Ed.* **2009**, *48*, 2500-2505.

(8) Hodgson, S. A.; Adamson, J.; Hunt, S. J.; Cliffe, M. J.; Cairns, A. B.; Thompson, A. L.; Tucker, M. G.; Funnell, N. P.; Goodwin, A. L., Negative area compressibility in silver(i) tricyanomethanide. *Chem. Commun.* **2014**, *50*, 5264-5266.

(9) DeVries, L. D.; Barron, P. M.; Hurley, E. P.; Hu, C.; Choe, W., "Nanoscale Lattice Fence" in a Metal–Organic Framework: Interplay between Hinged Topology and Highly Anisotropic Thermal Response. *J. Am. Chem. Soc.* **2011**, *133*, 14848-14851.

(10) Grobler, I.; Smith, V. J.; Bhatt, P. M.; Herbert, S. A.; Barbour, L. J., Tunable Anisotropic Thermal Expansion of a Porous Zinc(II) Metal–Organic Framework. *J. Am. Chem. Soc.* **2013**, *135*, 6411-6414.

(11) Aggarwal, H.; Das, R. K.; Engel, E. R.; Barbour, L. J., A five-fold interpenetrated metal–organic framework showing a large variation in thermal expansion behaviour owing to dramatic structural transformation upon dehydration–rehydration. *Chem. Commun.* **2017**, *53*, 861-864.

(12) Goodwin, A. L.; Calleja, M.; Conterio, M. J.; Dove, M. T.; Evans, J. S. O.; Keen, D. A.; Peters, L.; Tucker, M. G., Colossal Positive and Negative Thermal Expansion in the Framework Material $Ag_3[Co(CN)_6]$. *Science* **2008**, *319*, 794-797.

(13) Ogborn, J. M.; Collings, I. E.; Moggach, S. A.; Thompson, A. L.; Goodwin, A. L., Supramolecular mechanics in a metal–organic framework. *Chem. Sci.* **2012**, *3*, 3011-3017.

(14) Kondo, A.; Maeda, K., Anisotropic thermal expansion of a 3D metal–organic framework with hydrophilic and hydrophobic pores. *J. Solid State Chem.* **2015**, *221*, 126-131.

(15) Liu, Z.; Liu, C.; Li, Q.; Chen, J.; Xing, X., Spring-like motion caused large anisotropic thermal expansion in nonporous $M(eim)_2$ (M = Zn, Cd). *Phys. Chem. Chem. Phys.* **2017**, *19*, 24436-24439.

(16) Zhou, H.-L.; Lin, R.-B.; He, C.-T.; Zhang, Y.-B.; Feng, N.; Wang, Q.; Deng, F.; Zhang, J.-P.; Chen, X.-M., Direct visualization of a guest-triggered crystal deformation based on a flexible ultramicroporous framework. *Nat. Commun.* **2013**, *4*, 2534.

(17) Henke, S.; Schneemann, A.; Fischer, R. A., Massive Anisotropic Thermal Expansion and Thermo-Responsive Breathing in Metal–Organic Frameworks Modulated by Linker Functionalization. *Adv. Funct. Mater.* **2013**, *23*, 5990-5996.

(18) Hu, J.-X.; Xu, Y.; Meng, Y.-S.; Zhao, L.; Hayami, S.; Sato, O.; Liu, T., A Material Showing Colossal Positive and Negative Volumetric Thermal Expansion with Hysteretic Magnetic Transition. *Angew. Chem. Int. Ed.* **2017**, *56*, 13052-13055.

(19) Hunt, S. J.; Cliffe, M. J.; Hill, J. A.; Cairns, A. B.; Funnell, N. P.; Goodwin, A. L., Flexibility transition and guest-driven reconstruction in a ferroelastic metal–organic framework. *CrystEngComm* **2015**, *17*, 361-369.

(20) Yao, Z.-S.; Guan, H.; Shiota, Y.; He, C.-T.; Wang, X.-L.; Wu, S.-Q.; Zheng, X.; Su, S.-Q.; Yoshizawa, K.; Kong, X.; Sato, O.; Tao, J., Giant anisotropic thermal expansion actuated by thermodynamically assisted reorientation of imidazoliums in a single crystal. *Nat. Commun.* **2019**, *10*, 4805.

(21) Das, D.; Jacobs, T.; Barbour, L. J., Exceptionally large positive and negative anisotropic thermal expansion of an organic crystalline material. *Nat. Mater.* **2010**, *9*, 36-39.

(22) Fortes, A. D.; Suard, E.; Knight, K. S., Negative Linear Compressibility and Massive Anisotropic Thermal Expansion in Methanol Monohydrate. *Science* **2011**, *331*, 742-746.

(23) Engel, E. R.; Smith, V. J.; Bezuidenhout, C. X.; Barbour, L. J., Thermoresponsive Organic Inclusion Compounds: Modification of Thermal Expansion Behavior by Simple Guest Replacement. *Chem. Mater.* **2016**, *28*, 5073-5079.

(24) Liu, H.; Gutmann, M. J.; Stokes, H. T.; Campbell, B. J.; Evans, I. R.; Evans, J. S. O., Supercolossal Uniaxial Negative Thermal Expansion in Chloranilic Acid Pyrazine, CA-Pyz. *Chem. Mater.* **2019**, *31*, 4514-4523.

(25) Huang, Y.-G.; Shiota, Y.; Wu, M.-Y.; Su, S.-Q.; Yao, Z.-S.; Kang, S.; Kanegawa, S.; Li, G.-L.; Wu, S.-Q.; Kamachi, T.; Yoshizawa, K.; Ariga, K.; Hong, M.-C.; Sato, O., Superior thermoelasticity and shape-memory nanopores in a porous supramolecular organic framework. *Nat. Commun.* **2016**, *7*, 11564.

(26) van der Lee, A.; Roche, G. H.; Wantz, G.; Moreau, J. J. E.; Dautel, O. J.; Filhol, J.-S., Experimental and theoretical evidence of a supercritical-like transition in an organic semiconductor presenting colossal uniaxial negative thermal expansion. *Chem. Sci.* **2018**, *9*, 3948-3956.

(27) Panda, M. K.; Centore, R.; Causà, M.; Tuzi, A.; Borbone, F.; Naumov, P., Strong and Anomalous Thermal Expansion Precedes the Thermosalient Effect in Dynamic Molecular Crystals. *Sci. Rep.* **2016**, *6*, 29610.